Water Research 308 (2027) 126745

Contents lists available at ScienceDirect

Water Research

journal homepage: www.elsevier.com/locate/watres

Dose-dependent duality: Extracellular vesicles shift from metabolic facilitators to cytotoxic effectors during anaerobic denitrification

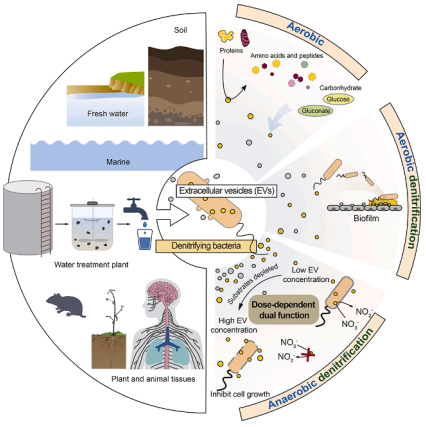
Yuzhen Ming [a,b], Wengen Zhu [a], Huanping Liu [a], Zuyuan Gao [a,b], Shiwei Xiao [b], Lanlan Cai [c], Xuyan He [a], Yusong Guo [d], Jizhong Zhou [e], Zhili He [a], Qinglu Zeng [b,*], Qingyun Yan [a,*]

[a] Marine Synthetic Ecology Research Center, Southern Marine Science and Engineering Guangdong Laboratory (Zhuhai), Zhuhai, 519082, China
[b] Department of Ocean Science, The Hong Kong University of Science and Technology, Clear Water Bay, Hong Kong, 999077, China
[c] Earth, Ocean and Atmospheric Sciences Thrust, The Hong Kong University of Science and Technology (Guangzhou), Guangzhou, 511453, China
[d] Division of Life Science, The Hong Kong University of Science and Technology, Clear Water Bay, Hong Kong, 999077, China
[e] Institute for Environmental Genomics, University of Oklahoma, Norman, OK, 73072, USA

HIGHLIGHTS

- Oxygen and nitrate levels drive functionally heterogeneous EV production.
- EVs show a dose-dependent shift from metabolic allies to cytotoxic effectors.
- EVs act as effector carriers lacking intrinsic denitrification activity.
- Biogenic nanoparticulates withstand sequential water purification barriers.

GRAPHICAL ABSTRACT



ARTICLE INFO

Keywords:
Extracellular vesicles
Denitrification
Pseudomonas aeruginosa
Virulence
Oxygen

ABSTRACT

Extracellular vesicles (EVs) mediate critical intercellular interactions, yet their special functions in anaerobic denitrification process remain poorly understood. Utilizing the model denitrifier *Pseudomonas aeruginosa* PAO1, we investigated how environmental oxygen and nitrate gradients reprogram vesicular cargo and functionality. Proteomic profiling revealed a clear condition-specific cargo: aerobically generated EVs selectively packaged virulence factors and nutrient acquisition proteins. In contrast, imposing severe bioenergetic stress via anaerobic denitrification forced a radical compositional inversion, driving a targeted accumulation of with peptidoglycan-degrading enzymes. Functionally, these EVs exhibited a dose-dependent duality. At physiological EV-to-cell ratios, they facilitated transient denitrification activity and early growth in recipient cohorts. Crossing a critical density threshold, however, they transitioned to cytotoxic effectors, suppressing culture density through a cytotoxic activity that emerged post-denitrification. Notably, despite carrying a full suite of denitrification

* Corresponding authors.
E-mail addresses: zeng@ust.hk (Q. Zeng), yanqingyun@sml-zhuhai.cn (Q. Yan).

https://doi.org/10.1016/j.watres.2026.126745
Received 21 April 2026; Received in revised form 23 July 2026; Accepted 14 August 2026
Available online 17 August 2026
0043-1354/© 2026 Elsevier Ltd. All rights are reserved, including those for text and data mining, AI training, and similar technologies.

enzymes, purified EVs displayed no intrinsic activity, indicating their primary roles is that of effector carriers rather than independent catalytic units. Furthermore, a substantial fraction of these bioactive nanoparticulates survived sequential multi-barrier municipal drinking water purification processes. Together, these findings redefine EVs not merely as condition-regulated ecological regulators during severe bioenergetic stress, but also as structurally recalcitrant colloidal entities within engineered aquatic environments.

1. Introduction

Cells across all domains of life actively secrete extracellular vesicles (EVs) into their environment (Gill et al., 2019), indicating that EV production is a fundamental and evolutionarily conserved biological process. EVs have been found to contribute to various biological processes, including virulence (Fonseka and Mathivanan, 2023), quorum signaling (Morinaga et al., 2018), nutrient acquisition (Salvachúa et al., 2020), biofilm formation, cellular defense, and horizontal gene transfer (Brito, 2021). The release of EVs is influenced by various environmental factors such as cultivation media, temperature, UV exposure, iron availability, oxygen availability, and antibiotic stress (Orench-Rivera and Kuehn, 2016; Schatz et al., 2021; Tashiro et al., 2010; Toyofuku et al., 2019; Zarantonello et al., 2018). These different factors induce EV formation via various biogenesis routes and lead to different types of EVs. For example, antibiotics that cause membrane perturbation mainly induce EV formation through membrane blebbing (Manning and Kuehn, 2011; Toyofuku et al., 2017). Another example is that DNA-damaging factors can induce EV formation through explosive cell lysis (Turnbull et al., 2016) and bubbling cell death (Toyofuku et al., 2017). These various types of EVs have distinct structures and contents, which affect their functions (Toyofuku et al., 2023). Since bacterial EVs typically range from 40 to 400 nm (Toyofuku et al., 2019), they may pass through standard water purification systems, making it challenging to completely remove EVs from drinking water.

EVs carry a variety of biological compounds that are thought to be selectively packaged as cargos, and thus some researchers recognize EVs as a cell secretion system (Maphosa et al., 2023; Tkach and Théry, 2016; Xie et al., 2022). Pathogenic bacteria produce EVs that contain microbe-associated immunogenic cargos, such as lipopolysaccharide (LPS), peptidoglycan (PG), nucleic acids, as well as other cell wall components (Renelli et al., 2004; Vanaja et al., 2016). Additionally, a series of cell wall–degrading enzymes from EVs, such as xylanases, lipase, and pectin lyase, are also critical for inducing host immune responses (Feitosa-Junior et al., 2019; Nascimento et al., 2016; Solé et al., 2015). Intriguingly, several studies suggest that bacterial EVs may contain enzymes involved in nutrient degradation (Salvachúa et al., 2020; Iraci et al., 2017), potentially allowing EVs to perform specific enzymatic reactions independently. However, these studies grew bacterial cultures and used the pellets after ultracentrifugation as pure EVs, which are likely to contain many impurities, such as secreted protein aggregates and cell debris (Wang et al., 2024). Thus, the intrinsic metabolic capacities of EVs remain to be tested in highly purified EV samples.

Excess nitrogen loading has shaped microbial communities and contributed to a series of environmental issues, such as eutrophication and red tides. To alleviate these problems, microbial denitrification could reduce nitrate to dinitrogen gas, a crucial process for driving nitrogen cycling. *Pseudomonas aeruginosa* PAO1 is a typical denitrifying bacterium encoding all denitrifying enzymes. It is canonically assumed that oxygen needs to be depleted before facultatively anaerobic organisms use nitrate as alternative electron acceptors from the perspective of thermodynamics. However, electron competition during aerobic denitrification is widely reported due to the branched respiratory chain of microorganisms (Thomas et al., 1994; Yang et al., 2020). Toyofuku et al. (2014) showed that PAO1 produces more EVs under anaerobic denitrification compared to aerobic conditions, which was suggested to be related to the DNA damage stress induced by nitric oxide (NO). However, it is difficult to tell clearly which factors (oxygen or/and nitrate) affect EV abundance, and whether EVs play a role in denitrification remains unclear.

In the current study, we used PAO1 to examine how denitrifying conditions influence the production and function of bacterial EVs. We tested the hypothesis that EVs mediate intercellular interactions during denitrification. Our study reveals that environmental cues prompt cells to modulate not only EV abundance but also their protein cargo and functional properties, with anaerobic denitrifying EVs exhibiting unique compositional and behavioral characteristics. Transitioning from microbial ecology to engineered infrastructure, we further evaluate the biophysical resilience of these biogenic nanostructures. Bench-scale simulations indicate that a substantial fraction of these active colloidal entities survives sequential, multi-barrier water purification processes. This robust physical persistence redefines EVs as highly recalcitrant environmental biocolloids, introducing a non-cellular dimension to particulate attenuation in engineered aquatic systems.

2. Materials and methods

2.1. Bacterial cultivation

The strains *P. aeruginosa* PAO1, *Stutzerimonas degradans* D4-6, and *P. alloputida* S1-7 were routinely maintained at 35 °C in Luria-Bertani (LB) medium or LB plates aerobically. For anaerobic cultures, PAO1 was inoculated in 100 mL bottles with 50 mL LB medium. The LB medium was supplemented with KNO_3 (7.1 mM, 50 mM, or 100 mM) or with 40 mM arginine for fermentation experiments, as described previously (Gamper et al., 1991; Vander Wauven et al., 1984). The concentration of 7.1 mM (equal to 100 mg N L^{-1}) KNO_3 was selected as it is widely used for bioreactors to test microbial nitrogen removal ability (Chung et al., 2014; Zhang et al., 2022). The highest KNO_3 concentration (100 mM) was chosen in line with previous study indicating enhanced EV production under anaerobic denitrification at this level (Toyofuku et al., 2014). The air within butyl-rubber-sealed Erlenmeyer flasks was replaced with argon by flushing argon (Ar) gas through a needle. The cells were cultured at 35 °C with shaking at 120 rpm. To prepare fresh culture for periodic sampling experiments, we grew the cultures at desired conditions for 24 h before inoculation into the fresh medium at a ratio of 1:100.

2.2. Enumeration of bacterial cells by flow cytometry

For bacterial cell count by flow cytometry, 1 mL cultures were collected at each time point. Cells were fixed at a final concentration of 1% glutaraldehyde for 15 min and frozen at −20 °C. Before flow cytometry analysis, cells were thawed and stained with SYBR gold by incubating for 1 h at 37 °C. Samples were counted using a flow cytometer (CytoFLEX LX, Beckman Coulter) and analyzed by the CytExpert software (Beckman Coulter).

2.3. Nitrate and nitrite quantification

To measure nitrate and nitrite concentrations, we collected 1 mL cultures at each time point and filtered them through a 0.45 μm syringe filter to remove cells. The filtrates were stored at −20 °C and typically analyzed within two weeks. Samples were then tested using an ion chromatograph (Thermo Scientific™ Dionex™ ICS-6000) per the

manufacturer's protocol.

2.4. EV isolation and purification

2.4.1. Kinetic tracking of vesicle production

To quantify the EV concentration in growing cultures, triplicate 100 mL aerobic or 50 mL anaerobic cultures were grown as described above. At each time point, 2 mL cultures were collected and gently filtered through a 0.45 μm syringe filter to separate vesicular fraction from intact cells. The filtrate was frozen at −20 °C until NTA analysis. For cell samples, 1 mL samples were collected and fixed with 1% glutaraldehyde for flow cytometry analysis. The vesicle production rate at exponential phases was calculated according to previous studies (Biller et al., 2014), assuming that vesicle loss is negligible (Supplementary information).

2.4.2. EV purification for proteomic profiling

For proteomic analysis of EVs, triplicate 2 L cultures at stationary phase were centrifuged at 8000 × *g* for 30 min at 4 °C to pellet the cells. Then, the supernatant was filtered through 0.45 μm vacuum filter membranes to remove the remaining bacteria. Tangential flow filters (100 kDa cutoff) connected to a peristaltic pump were utilized to concentrate filtrate to about 30 mL. Feed pressure was kept < 2 psi throughout processing. The concentrated supernatant was gently filtered through a 0.45 μm syringe filter to ensure no cells remained before ultracentrifugation at 100,000 × *g* (Beckman-coulter Type70Ti rotor, 1.5 h, 4 °C).

To further purify vesicles, the vesicle pellets were first suspended in 1.3 mL of 45% Optiprep™ (Serumwerk Bernburg AG, Germany) in a HEPES buffer containing 0.85% NaCl and 10 mM HEPES, pH 8, then placed in the bottom of 13.2 mL UltraClear ultracentrifuge tube (Beckman-coulter) and overlaid with equal volumes of 40%, 35%, 30%, 25%, 20%, 15%, 10% and 0% Optiprep (in the same background). The gradient tubes were ultracentrifuged at 200,000 × *g* for 2 h at 4 °C in a SW41Ti rotor (Beckman-coulter), and twelve fractions were collected. Electron microscopy was routinely used to confirm the content and purity of vesicle fractions. The vesicle fractions, after density gradient ultracentrifugation, were washed by diluting the samples with HEPES buffer (10 mM HEPES containing 0.85% NaCl) and pelleting them in an ultracentrifuge (100,000 × *g*, 1.5 h, 4 °C, Beckman-coulter Type70Ti rotor). The protein concentration and EV abundance from samples was then measured using Bradford Protein Assay Kit (Sangon Biotech, Shanghai, China). The details of experimental data have been submitted to the EV-TRACK knowledgebase (EV-TRACK ID: EV260061).

2.5. Nanoparticle tracking analysis (NTA)

EV concentration and size distribution were analyzed by NTA (Particle Metrix ZetaView). Samples were diluted in ddH_2O to a final volume of 1 mL. Pre-tests were conducted to find the ideal measurement concentration with sensitivity set to 80, shutter to 100, and frame rate to 30. Other parameters were followed as the manufacturer's default settings. For each measurement, three cycles were performed by scanning 11 cell positions and capturing 30 frames per position. After capture, the videos were analyzed with the maximum area set to 1000, minimum area set to 5, and minimum brightness set to 25. All data files were processed with identical settings. The mode size values, which are calculated from the diameter values of the most abundant particle class, were selected to represent the vesicle diameter of each sample and avoid the impact of outliers in the tails of the distribution.

2.6. Transmission electron microscope (TEM)

Purified EV samples (5 μL) were applied to a freshly charged formvar-coated copper grid and stained with uranyl acetate for 1 min. The grid was then briefly washed with ddH_2O for 1 min and allowed to dry. Grids were imaged on a JEM-1400 electron microscope (JEOL Ltd., Japan). EV samples after density gradient ultracentrifugation were imaged to confirm vesicle morphology and purity.

2.7. Proteomics analysis

Purified EV samples were processed for label-free quantitative (LFQ) proteomics by Novogene Bioinformatics Technology Co. Ltd. (Beijing). Samples were subjected to in-solution tryptic digestion in 100 mM TEAB buffer at 37 °C for 4 h. Then, the resulting peptide fragments were separated by NanoElute ultra-high-performance liquid chromatography (UHPLC) and analyzed by the tims-TOF Pro2 mass spectrometry.Raw spectral data and LFQ quantification were processed by MaxQuant software environment. The protein annotation was based on the *P. aeruginosa* PAO1 UniProt database (strain 1766024, 5643 sequences). Mitigating false-positive inflation within biological triplicates necessitated stringent data filtering. Specifically, only peptide spectrum matches (PSMs) with >99% confidence were accepted. Subsequent protein identification strictly required the presence of at least one unique peptide. Initial functional ontology was assigned using InterProScan (v. 5.22–61.0) for GO terms (Jones et al., 2014), while KEGG pathways and COG (Cluster of Orthologous Groups) categories were mapped via BLAST (v. 2.2.26) applying a strict *e*-value cutoff of $\leq 1 \times 10^{-5}$.

Downstream statistical computing and data visualization were performed in the R statistical environment. To address the variance inherent in vesicular cargo and the statistical constraints of a triplicate matrix, LFQ intensities were $\log_2$-transformed prior to comparative analysis. Differentially expressed proteins (DEPs) between metabolic treatments were delineated applying a strict a priori threshold of an absolute fold-change ≥ 1.5 (or ≤ 0.67 for downregulation) coupled with a statistical significance of $p < 0.05$. Functional enrichment analysis of curated DEPs was performed by the DAVID functional annotation server (https://david.ncifcrf.gov/home.jsp) (Sherman et al., 2022). The mass spectrometry proteomics data have been deposited to the ProteomeXchange Consortium (https://proteomecentral.proteomexchange.org) with the dataset identifier PXD054578.

2.8. Extracellular vesicles co-culture assays

Source EVs were derived from *P. aeruginosa* PAO1 cultures cultivated to the late exponential growth phase under three conditions: aerobic non-denitrification, aerobic denitrification (with 7.1 mM NO_3^-), and anaerobic denitrification (with 7.1 mM NO_3^-). Following harvest and purification (detailed in Section 2.4.2), biogenic EVs were absolutely quantified utilizing NTA and standard protein assays. For the challenge assay, three distinct recipient lineages—autologous *P. aeruginosa* PAO1, alongside heterologous *S. degradans* D4-6, and *P. alloputida* S1-7—were inoculated into fresh media at a 1:50 ratio under three conditions. These newly transferred communities were immediately supplemented with the purified EVs. We strictly matched the physiological origin of the vesicular cargo to the recipient's specific incubation environment. Isopycnic HEPES buffer served as the negative control.

Aerobic cohorts were housed in standard 50 mL sterilized tubes. Anaerobic recipient cultures were maintained in Hungate tubes, sealed with butyl rubber stoppers, and continuously purged with argon (Ar) gas. The biogenic EVs and the corresponding negative controls (HEPES buffer) were injected into these anoxic vessels via sterile syringes.

To accurately simulate natural exposure, we applied specific EV-to-cell ratios derived from prior quantitative characterization data (Fig. 1): 25:1 for aerobic non-denitrification, 30:1 for aerobic denitrification, 100:1 for anaerobic denitrification co-cultures. All the mixtures were incubated at 35 °C with shaking at 120 rpm.

To assess the intrinsic metabolic capacity of EVs, purified EV samples alone were incubated with 20 mM NADH as an electron donor under denitrifying conditions (ON and N). Cell enumeration and NO_3^- / NO_2^-

quantification at each time point were performed as described above. EV-cell co-culture assays were not performed under the anaerobic fermentation with arginine condition, as *P. aeruginosa* PAO1 exhibited significant cell aggregation under this condition, precluding reliable cell enumeration (Vander Wauven et al., 1984).

2.9. Cell death quantification

Cell death in EV-bacteria co-cultures was assessed using acridine orange (AO) and ethidium bromide (EB) staining. AO permeates all cells and emits green fluorescence, while EB is only taken up by membrane-compromised cells, emitting red fluorescence by intercalation into DNA. Samples were taken after 6 h, 12 h, and 24 h of incubation and diluted to 1×10^6 cell mL^{-1} and stained with AO/EB solution for 15 min at room temperature according to the manufacturer's protocol. Dual fluorescence was visualized under a fluorescence microscope (Leica, DM6B). AO and EB were excited using 480 nm and 538 nm filters, respectively, and emission signals were collected at 530 nm (AO, green channel) and 610 nm (EB, red channel). In parallel, live and dead cells from each sample were quantified by flow cytometer (CytoFLEX LX, Beckman Coulter) with appropriate filter sets.

2.10. EVs-cell interaction assays

To visually track the physical association of EVs with recipient cells, we utilized the lipophilic membrane dye PKH67 (Fluorescence Biotechnology, Beijing, China) according to the manufacturer's protocol. First, the 100 μL of PKH67 dye was diluted in 900 μL of kit-supplied Diluent C to make a PKH67 working solution. This working solution was mixed with the purified EV samples at a 1:25 ratio and incubated at 37 °C for 5 min to allow for the labeling reaction, followed by washing with HEPES buffer (10 mM HEPES containing 0.85% NaCl) and pelleting in an ultracentrifuge (100,000 × *g*, 1.5 h, 4 °C, Beckman-coulter Type70Ti rotor). The PKH67-marked EV pellets were finally resuspended in HEPES buffer and ready for further incubation experiments.

Each labeled EV sample was subsequently incubated with bacterial cultures. To exclude false-positive fluorescence artifacts or the free dye partitioning into recipient cellular membrane, we processed a dye-only mock control through the identical washing and ultracentrifugation pipeline. After 24–48 h, the cultures were collected and fixed with 1% glutaraldehyde, spotted on a microscopic slide, and stained with DAPI staining solution. EVs and bacterial cell were analyzed and imaged separately using a laser confocal microscope (Stellaris 5, Leica Microsystems). PKH67-labeled EVs were visualized using an excitation wavelength of 490 nm with emission collected at 502 nm, while DAPI-stained cells were visualized using an excitation wavelength of 340 nm with emission collected at 450 nm.

2.11. Water purification treatments

To empirically assess the structural recalcitrance of vesicular colloids against engineered environmental barriers, we subjected purified EV samples from PAO1 cultures to a sequentially municipal water treatment cascade. The initial vesicular suspension was spiked to an absolute concentration of 9×10^9 particles mL^{-1}, consistent with the particle concentration under anaerobic denitrification. This titer conservatively mimics high-density localized loading events typical of biofilm sloughing or extreme aquatic blooms. The laboratory-scale protocol included flocculation and sedimentation, filtration, ion exchange, adsorption, and disinfection. Initial electrostatic destabilization was achieved by dosing 5% polyaluminium chloride (PAC) into each 500 mL water sample, immediately followed by rapid manual stirring with a sterile glass rod for 2 min. We subsequently introduced 0.3% polyacrylamide (PAM) as a bridging flocculant, transitioning the system to gentle, constant manual swirling for 15 min to facilitate floc growth while preventing shear-induced floc breakage. Flocculated aggregates were allowed a 30 min quiescent settling period. The clarified supernatant sequentially permeated through commercial water filters (SUPOR, China) for filtration, ion exchange, and adsorption steps, as stated in their product functional descriptions. Finally, the filtrate was disinfected with chlorine dioxide, at a standardized dosage of 2 mg L^{-1}. Following a strict contact time of 15 min, samples were immediately processed to arrest prolonged oxidative exposure. Absolute surviving particle titers across these sequential physical and chemical stressors were quantified directly via high-resolution NTA.

2.12. Statistical analysis

All statistical analyses were performed using R software (v. 4.1.2). Prior to hypothesis testing, the Shapiro test was first used to verify whether the data were normally distributed. For normally distributed data, significant differences among two groups were determined by Student's *t*-test, and among multiple groups by one-way ANOVA with post-hoc testing. The non-parametric tests (Dunn's test and Wilcoxon test for two groups and the Kruskal-Wallis test for multiple groups) were applied to evaluate the significant differences among groups with abnormal distribution.

3. Results

3.1. Oxygen and nitrate influence EV production in P. aeruginosa PAO1

Denitrification is an important cell respiratory pathway in which oxygen and nitrate serve as terminal electron acceptors, providing energy for various bacterial cellular activities (Kuypers et al., 2018; Ucar et al., 2017). The simultaneous respiration of NO_3^- and O_2 has been demonstrated in pure cultures and natural microbial communities (Chen et al., 2006; Marchant et al., 2017) . We first examined cell growth status and nitrate reduction activity without or with nitrate concentrations (0, 7.1, 50, and 100 mM) under aerobic and anaerobic conditions. Aerobic cell growth rates were significantly higher than anaerobic rates and were relatively unaffected by nitrate concentrations (Figs. 1**a-f, S1, S2**). In contrast, denitrification activities were more sensitive to nitrate concentration under anaerobic conditions, with the pronounced accumulation of nitrite in anaerobic cultures with higher nitrate loads (**Fig. S2**), indicating that while oxygen governs the absolute growth capacity, nitrate availability strictly modulates the kinetics of the anaerobic electron transport chain.

To approximate the vesiculation capacity across six treatments, we next quantified the bulk extracellular nanoparticle abundance (Fig. 1**a-f**). Particulate release was robust. Extracellular particles consistently outnumbered the intact PAO1 cells by at least an order of magnitude. Strikingly, both oxygen and nitrate significantly modulate the particulate accumulation. Anaerobic condition accelerated initial nanoparticle production during exponential phases and yield higher absolute counts at the stationary phase. This producing divergence peaked at the maximum nitrate load (100 mM), driving a ~2.49-fold increase in anaerobic particle abundance compared to aerobic baselines (Fig. 1**g, h**). The diameter of particles produced anaerobically was also significantly larger than that of aerobic samples at 7.1 and 100 mM nitrate (Fig. 1**i**). Furthermore, particle production rates correlated positively with nitrate concentrations (Pearson correlation, $R = 0.7$, $p < 0.05$). While stationary-phase particle counts also scaled with nitrate levels under anoxia, the correlation weakened considerably ($R = 0.3$, $p < 0.05$). Together, these results suggested that oxygen availability and high nitrate concentrations collectively drive increased production of larger nanoparticulate structures.

3.2. Oxygen and nitrate determine protein compositions in EVs of P. aeruginosa PAO1

To gain insight into how these environmental factors influence EV

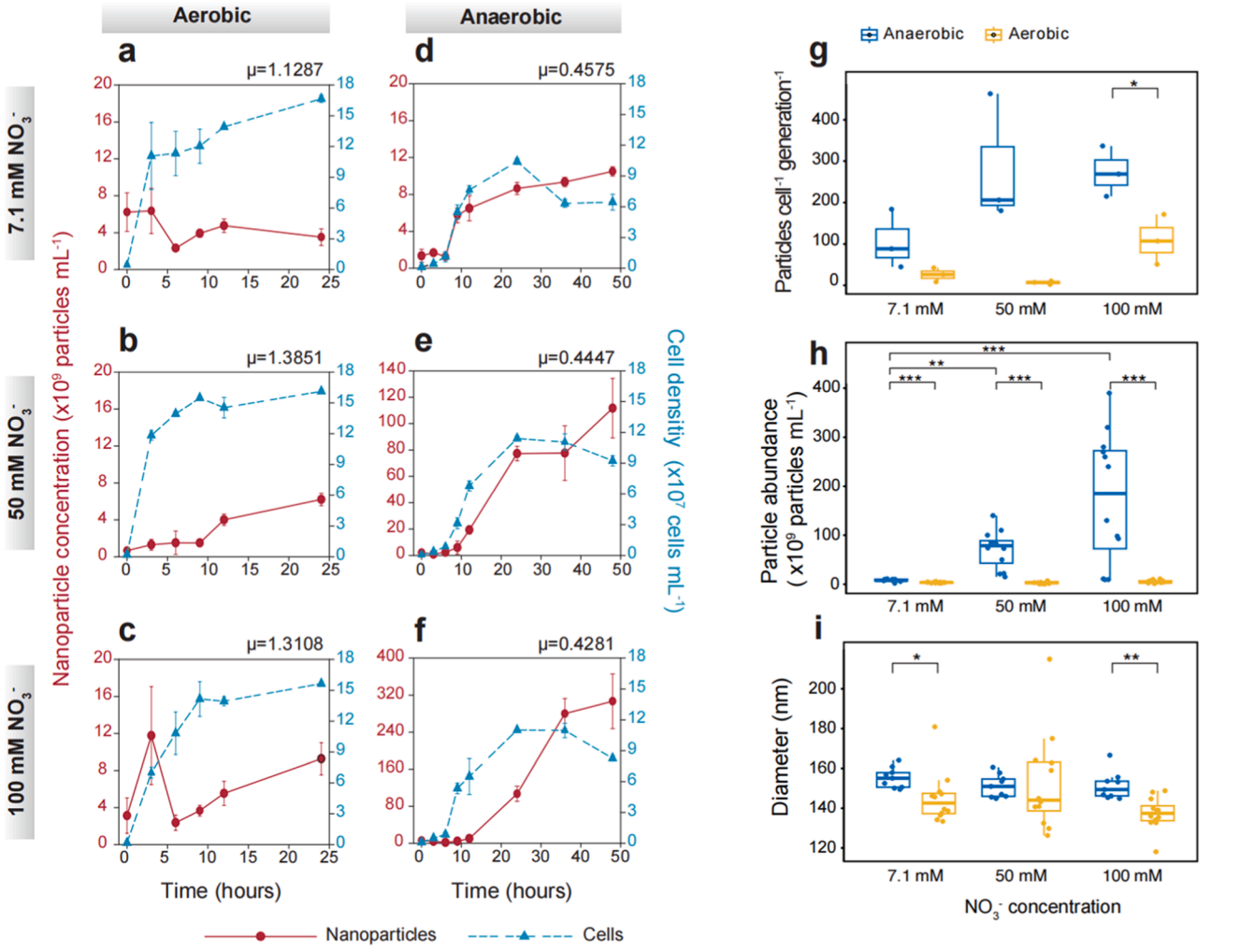


Fig. 1. Oxygen and nitrate availability dictate extracellular vesicle (EV) production dynamics in *P. aeruginosa* PAO1. a-f. Kinetic tracking of macroscopic growth alongside corresponding extracellular nanoparticles accumulation over time. Error bars represent the standard deviation from three independent experiments. Growth rates (μ, h^{-1}) were calculated by fitting a linear regression to the log-transformed values during the exponential growth phase (Supplementary information). The calculated growth rates under each treatment were displayed on the respective panel. **g.** EV production rates during exponential phases under different cultivation conditions. **h-i.** Particle abundance (**h**) and the peaks of particle diameters (**i**) during stationary phases in response to different oxygen and nitrate concentration. Statistical significance was evaluated independently according to data distribution constraints. Parametric two-group comparisons (panels g, i, and the 7.1 mM nitrate group in panel h) utilized a two-tailed unpaired Student's *t*-test. Where normality assumptions were violated, isolated two-group differences (the 50 and 100 mM nitrate groups in panel h) were assessed via the Wilcoxon rank-sum test. Variance across three non-parametric groups (panel h) was determined using the Kruskal-Wallis test coupled strictly with Dunn's post-hoc correction for multiple comparisons. *, $p < 0.05$; **, $p < 0.01$, ***, $p < 0.001$.

functions, we characterized the protein profiling of EVs under four key conditions: aerobic condition (type O), aerobic denitrification with 7.1 mM NO_3^- supplemented (type ON), and anaerobic denitrification with 7.1 mM NO_3^- supplemented (type N), anaerobic fermentation with arginine (type A). EV samples were rigorously purified by density gradient ultracentrifugation (**Fig. S3a**). EVs collected in aerobic cultures were found in lighter densities (1.12–1.15 g mL^{-1}) in light yellow or brown color (**Table S1**). In contrast, EVs from anaerobic samples fractionated to the heavier fractions (1.13–1.18 g mL^{-1}) in white color, suggesting a distinct biomolecular composition (**Figs. S3b, S4**).

Negative-stain transmission electron microscopy (TEM) confirmed the intact morphological structure of the isolated EV fractions (**Fig. S3c-e**). Complementary NTA profiling identified condition-specific size distributions, with predominant peaks emerging at, 150 nm (type O), 145 nm (type ON), and 152.5 nm (type N) (**Fig. S5**). To validate the analytical stringency of this isolation pipeline, we assessed the particle-to-protein ratio of the recovered EV fractions. The preparations yielded ratios spanning from 9.46×10^9 to 1.30×10^{11} particles μg^{-1} protein (**Table S2**). This physical metric indicates a highly purified vesicular suspension depleted of adventitious free protein complexes, aligning directly with established isolation quality standards (Webber and Clayton, 2013).

Proteomics analysis of EVs identified 311 unique proteins (**Table S3**). Multivariate ordination via Principal component analysis (PCA) revealed distinct, condition-dependent trajectories in cargo sorting. Notably, the arginine fermentation (type A) dataset segregated entirely from the respiratory regimes (Fig. 2**a**). Within the respiratory regimes, shifting towards denitrifying conditions (types ON and N) stimulated a broader packaging capacity, harboring a demonstrably expanded protein repertoire relative to strictly aerobic conditions. (Fig. 2**b**).

Subcellular localization prediction of 174 proteins confirmed typical Gram-negative bacterial EV features, with outer membrane, inner membrane, and cytoplastic proteins being highly represented (Figs. 2**c, S6, Table S4**). Across the specific respiratory gradients (type O, ON, and N), outer membrane proteins consistently constituted the largest structural fraction. Interestingly, the transition from aerobic respiration to anaerobic denitrification correlated with a progressive structural

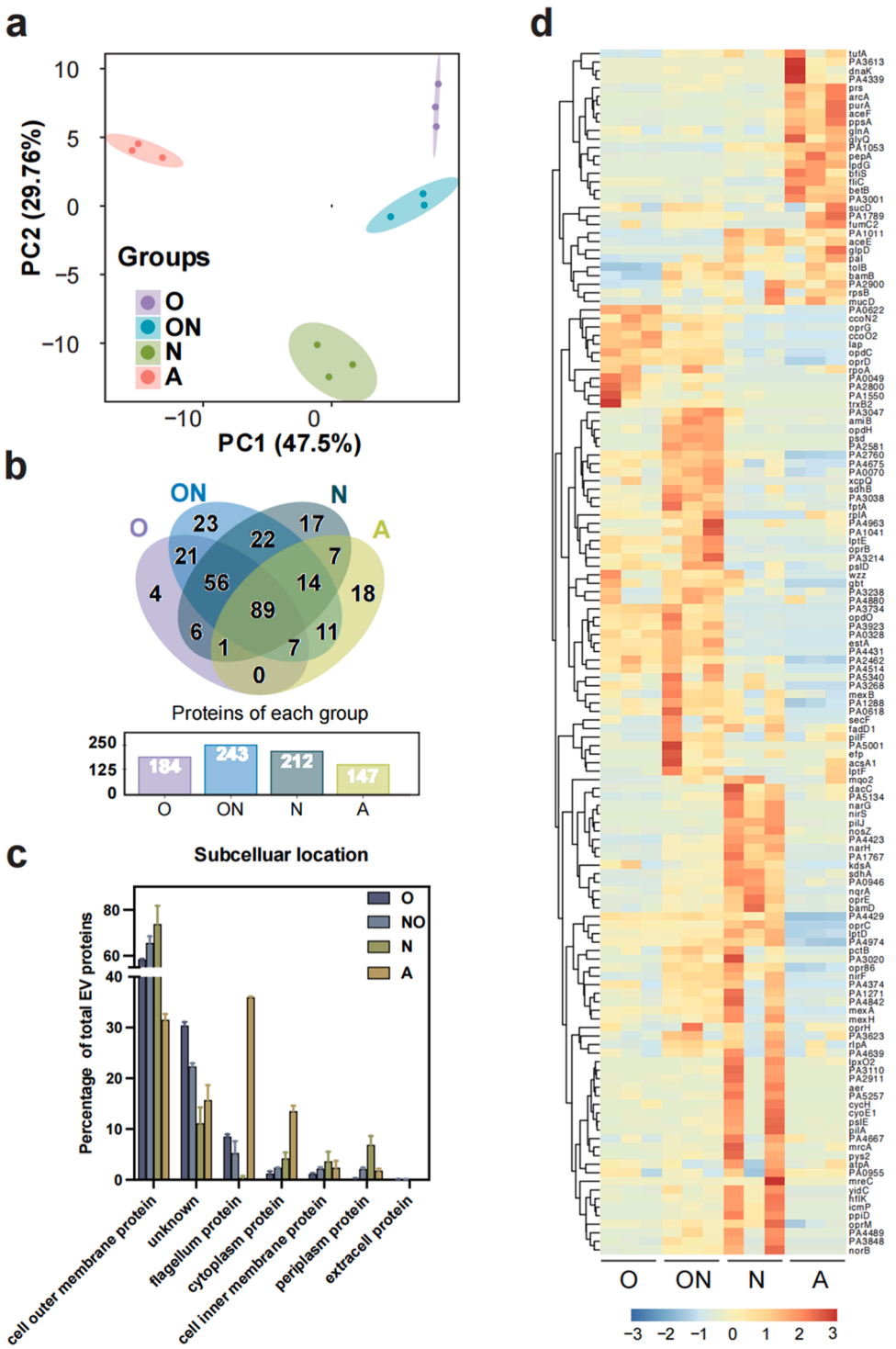


Fig. 2. Quantitative mass spectrometry analysis of extracellular vesicles (EVs) proteome from different cultivations. a. PCA analysis of the quantitative comparison shows a clear separation in protein components of four types of samples. **b.** Venn diagram showing the distribution of proteins qualitatively identified in four types of samples by peptides in at least two of three replicates. **c.** The different abundance ratio of proteins with different subcellular location. The values represent the relative percentage of proteins from a specific localization category within the total annotated proteins for that specific sample. **d.** Multi-group comparison showed that 141 proteins were differentially expressed. Three (n = 3) independent biological replicates per treatment. Abbreviation: A, EVs samples from anaerobic cultures with arginine addition; N, EVs samples from anaerobic cultures with 7.1 mM NO_3^- supplemented; NO, EVs samples from aerobic cultures with 7.1 mM NO_3^- supplemented; O, EVs samples from aerobic cultures without NO_3^- supplemented.

enrichment of outer membrane protein, inner membrane protein, and periplasm protein (**Fig. S6, Table S4**). In contrast to the respiratory fractions, the protein profile of arginine fermentation EVs was unique, notably enriched with the flagellum protein (FliC) and cytoplasm proteins (**Fig. S6**). This dramatic compositional shift suggests that anaerobic fermentation likely triggers an alternative, stress-induced membrane vesiculation pathway.

3.3. Enrichment analysis reveals differentially enriched functions of EVs in response to oxygen and nitrate stress

Vesicular proteomes undergo significant compositional remodeling under distinct physicochemical regimes. A multi-group comparison showed that 141 proteins were differentially expressed among the samples (Figs. 2**d, S7, Table S5**) ($p < 0.05$, fold-change ≤ 0.67, or ≥ 1.5).

EVs under aerobic conditions (type O and type ON) are enriched in proteins with predicted roles in porin activity, metalloexopeptidase activity, and cell motility (Figs. 3**, S7, Tables S5 and S6**). This cargo profile putatively equips EVs for extracellular matrix remodeling and opportunistic nutrient scavenging. Within the strictly aerobic cohort (regime O), enrichment was heavily skewed toward nutrient transporters. Specifically, the accumulation of OprD, OprB, and OpdO indicates a structural readiness for the uptake of gluconate, basic amino acids, and peptides (Chevalier et al., 2017; Huang and Hancock, 1993; Trias and Nikaido, 1990; Wylie and Worobec, 1995). Concurrently, aerobic EVs accumulated Lap and PA0328. These metalloexopeptidases cleave terminal peptide bonds, liberating free amino acids for metabolic integration. OprD is also widely reported to serve as the entry of antibiotics, especially imipenem and meropenem (Quinn et al., 1991; Yoneyama et al., 1995). Numerous uniquely enriched functions were in the aerobic denitrifying EV samples (type ON). Notably, the virulence-associated factors were even more up-regulated (DacC (Pal et al., 2024), EstA (Kang et al., 2009), LptF (Cheng et al., 2023), OprE (Rebière-Huët et al., 2002), OpdH (Tamber et al., 2007), PA2760 (Arhin and Boucher, 2010), PilA (Farinha et al., 1993), PilF (Koo et al., 2008)) in aerobic denitrification between the comparison of these two groups (**Figs. S7, S8, Table S5**).

Transitioning to denitrifying conditions (regimes ON and N) fundamentally rewired the vesicular inventory. Enrichment shifted abruptly toward protein insertion into membrane, lytic endotransglycosylase activity, nitrogen metabolism, microbial metabolism in diverse environments, and citrate cycle. Specifically, the robust accumulation of RlpA and AmiB points toward localized peptidoglycan degradation capabilities (Jorgenson et al., 2014). EV proteins from anaerobic denitrification (type N) were uniquely enriched in cell division, and glycolysis (Figs. 3**, S8, Tables S6 and S7**). Notably, almost all the denitrification enzymes were detected under anerobic denitrification (NarG, NarH, NarK2, NirS, NirQ, NirF, NorB, NorC, NosZ and NosR). This indicated their potential for involvement in this process.

3.4. EVs from anaerobic denitrification exhibit dose-dependent, dual effects on bacterial growth and denitrification

Given the enrichment of cytotoxic and metabolic enzymes in EVs isolated from cells under denitrifying conditions, we investigated the functional impact of EVs on bacterial cultures. We co-cultured purified EVs from anaerobic denitrification with host strain (PAO1), a denitrifying strain (*S. degradans* D4-6) and a non-denitrifying strain (*P. alloputida* S1-7) isolated from a nitrogen-removal bioreactor. The status of marked bacteria and EVs were checked first, as well as the dye-only control (**Fig. S9**). Confocal microscopy confirmed that PKH67-labeled EV co-localized with all three strains (Fig. 4**a-c**), demonstrating interspecies interaction potential.

Initial experiments using a high EV concentration (35 μg mL^{-1} protein) revealed a complex phenotype: EV addition led to a suppression of the initial denitrification rate and resulted in a lower final culture density in denitrifying strain (PAO1) (**Fig. S10**). We hypothesized this was due to a dose-dependent duality, where EVs might deliver beneficial enzymes at low concentrations but exert cytotoxic effects at high concentrations. To test this, we repeated co-cultures using lower, physiologically relevant EV-to-cell ratios (100:1, equivalent to 4.95 μg mL^{-1} protein EVs). At these low ratios, the same EVs enhanced denitrification rates and promoted early exponential growth. Despite this initial beneficial effect, they still significantly suppressed the final cell density in the stationary phase, consistent with our initial observations (Fig. 4**d-f**).

This growth suppression was mechanistically linked to EV-induced cell death. Flow cytometric quantification of live/dead cells revealed that anaerobic denitrifying EVs caused a substantial increase in cell

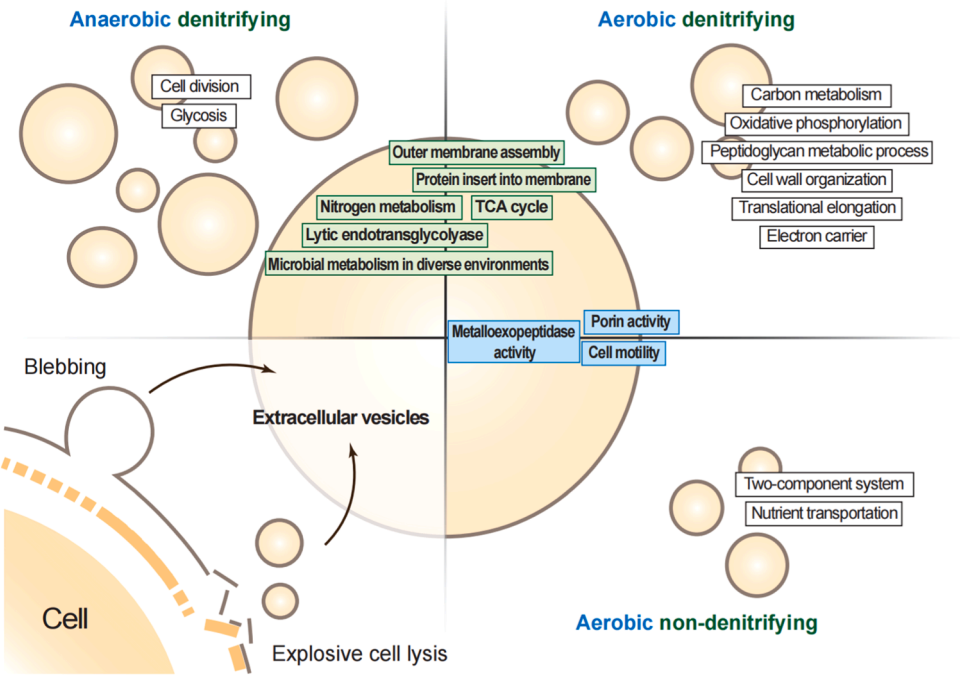


Fig. 3. Summary of enriched protein function under different conditions. Assignment of the protein functions under different conditions are analyzed based on the proteins significantly up regulated in each sample. EVs are schematized as lipid bilayer (thick brown circles) release from cell by blebbing or explosive cell lysis. Protein functions with green background are enriched in aerobic and anaerobic denitrifying conditions; blue background denote the functions enriched under aerobic conditions with or without nitrate supplemented; white background denotes the functions uniquely enriched in corresponding conditions.

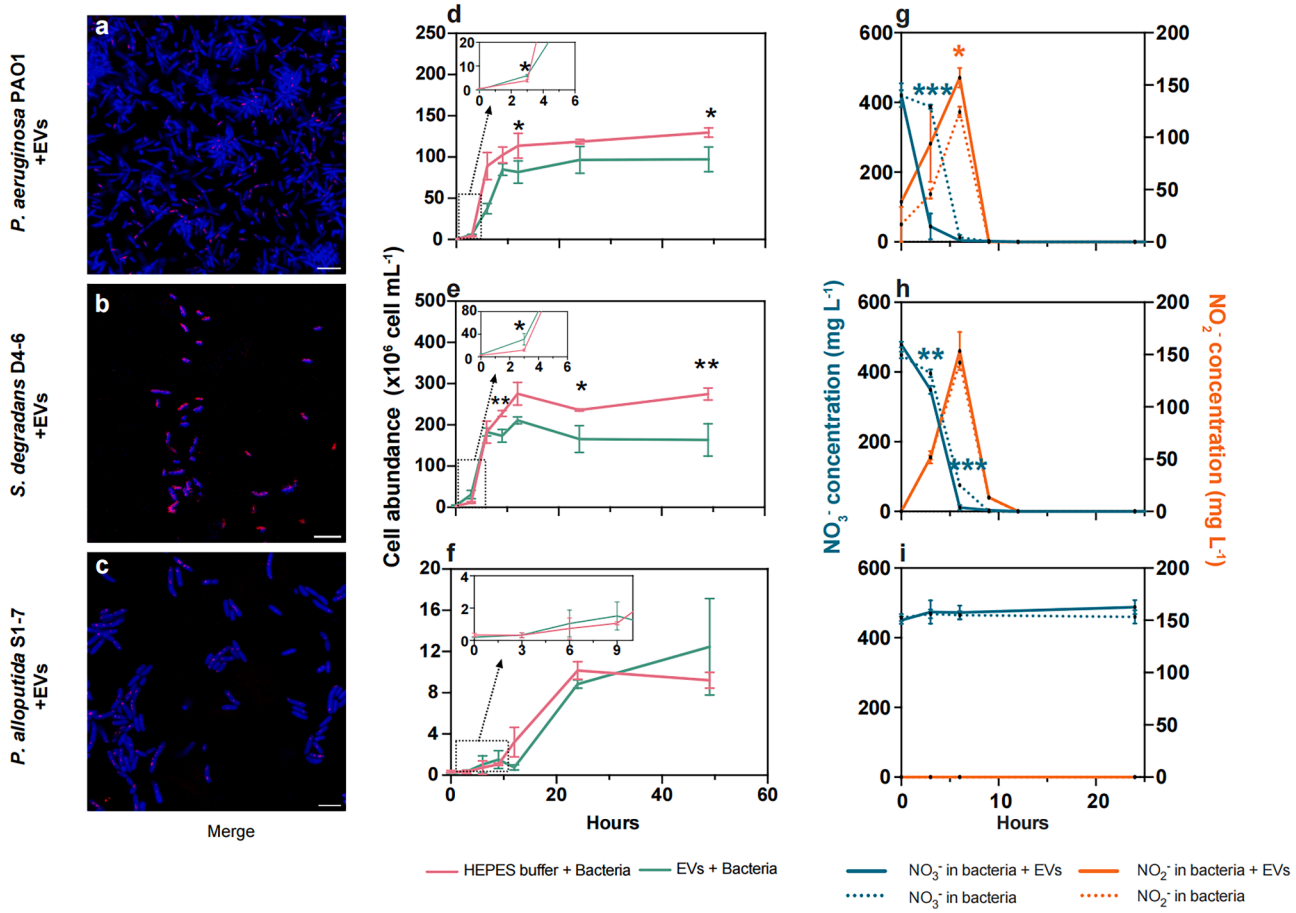


Fig. 4. EVs interaction with host cell (*Pseudomonas aeruginosa* PAO1), denitrifying strain (*Stutzerimonas degradans*D4-6) and non-denitrifying strain (*P. alloputida* S1-7) under anaerobic denitrification. a-c. Extracellular vesicles (EVs) were collected from *P. aeruginosa* PAO1 under anaerobic denitrifying conditions. After being washed with HEPES buffer, EVs were labeled with PKH67 dye (pseudocolored red) and supplemented in three strains. Cultures were collected and marked with DAPI dye (blue fluorescence) for further confocal microscopy observation after 48-h-incubation (scale bar = 5 μm). **d-f.** Growth profiles of three strains with EVs addition (the ratio of EVs to cells is about 100:1) under anaerobic denitrifying conditions. **g-i.** Concentration of nitrate and nitrite during bacterial incubation. Statistical significance across all quantitative panels was determined via two-tailed unpaired Student's *t*-tests, comparing EV-treated cohorts directly against their concurrent controls at discrete time points; *, $p < 0.05$; **, $p < 0.01$, ***, $p < 0.001$.

death, with the proportion of dead cells rising from approximately 30% in controls to over 70% in EV-treated cultures after 24 h of co-incubation (**Fig. S11**). This increase in mortality coincided with the onset of growth inhibition, suggesting that the observed reduction in final culture density is driven, at least in part, by EV-mediated cytotoxicity.

This cytotoxic effect was more pronounced in denitrifying bacteria. EVs from aerobic conditions (O) also exert a significant growth suppression, although it is less potent, and manifests later (around 24 h) compared to the anaerobic denitrifying EVs (**Figs. S12, S13**). Most intriguingly, EVs produced under aerobic denitrification (ON)—where cells utilize both oxygen and nitrate—showed the weakest bactericidal activity and did not significantly inhibit growth (**Figs. S11, S13**).

Strikingly, despite the packaging of a nearly complete set of denitrification enzymes (NarG, NirS, NorB, NosZ, etc.) in anaerobic denitrifying EVs, the isolated fractions failed to catalyze independent nitrate reduction *in vitro* (**Fig. S14**). This inert phenotype persisted even when EVs were administered at the precise physiological dosage (equivalent to the 100:1 EV-to-cell ratio) proven to drive the macroscopic growth and metabolic shifts in the intact co-cultures. The complete absence of cell-free catalytic activity under identical exposure constraints suggests the primary role of EVs is not as independent metabolic units but as carriers of effector molecules.

3.5. Biophysical resilience of nanoparticulate structures under stimulated drinking water purification process

Finally, given the identified numerous pathogenic effectors (e.g., LPS, porins) in EVs, we evaluate their persistence in drinking water. We simulated the public drinking water treatment process (flocculation, sedimentation, filtration, ion exchange, absorption, disinfection) in laboratory using purified EV samples from PAO1. High-resolution NTA tracked the colloidal stability of the nanoparticulates through these successive barriers. Particle abundance exhibited a cumulative, stepwise decline across the purification stages. approximately half of the EVs remained, with a residual rate of 44.98±9.81% (Fig. 5). This robust physical persistence indicated that biogenic colloidal structures endure conventional engineered environmental stressors.

4. Discussion

P. aeruginosa PAO1 dynamically regulates EV biogenesis in response to environmental oxygen and nitrate. These biogenic nanoparticulates operate as active, condition-dependent mediators of bacterial ecology (Fig. 6). Extending these biophysical parameters to engineered systems, we mapped the structural recalcitrance of these EVs against conventional water purification systems. Integrating these metabolic and physical metrics provides a revised framework for understanding

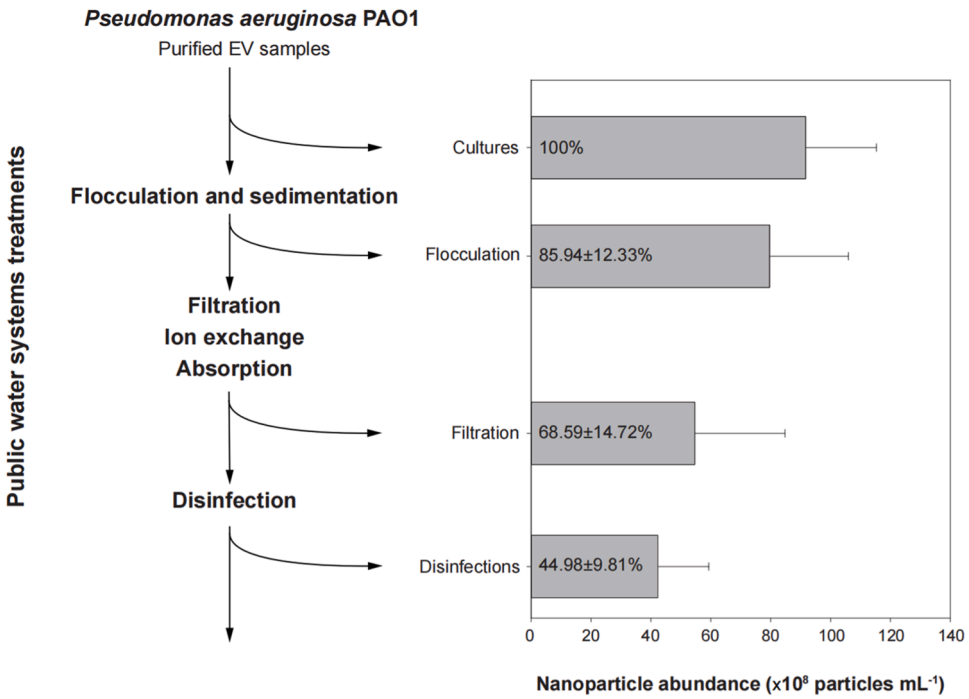


Fig. 5. Nanoparticle abundance detected during water treatment processes. Purified EV samples from PAO1 cultures were used to simulate the public drinking water treatment process, which included flocculation and sedimentation, filtration, ion exchange, absorption, disinfection. The bar plot illustrates the particle abundance in the samples after each treatment step. The residual rate of nanoparticles in each sample was calculated by comparing the abundance with that of the raw samples.

vesicular dynamics in constrained microenvironments.

A central finding is the condition-specific functional diversification of EV cargo. Aerobically generated fractions exhibited lower buoyant densities and distinct light yellow-brown pigmentation. This macroscopic phenotype likely reflects the co-segregation of reaction products of pyocyanin with thiol-containing metabolites like glutathione (Cheluvappa et al., 2008). Interpreting this shift demands analytical restraint. The relatively constrained number of identified vesicular proteins reflects highly selective physical packaging rather than stochastic cellular leakage. While our triplicate ($n = 3$) profiling restricts the statistical resolution of subtle abundance fluctuations, this limitation deliberately directs our mechanistic focus toward extreme compositional inversions. A primary example is the massive enrichment (7.31 to 9.91-fold) of RlpA in anaerobic EVs. Occurring despite its reported low cellular expression under hypoxia (Kamath et al., 2017), this asymmetric accumulation presents a dual hypothesis: a stress-induced disposal route for excess proteins, or a targeted delivery system aimed at modifying cell wall integrity. Our co-localization assays strongly support the latter. Differentiating transient surface docking from active membrane fusion, however, remains optically unresolved. Regardless of the exact internalization mechanics, visual data confirm that PAO1 EVs successfully docked with autologous cells and across distinct intra-generic and intra-familial lineages. Within multi-species biofilms, these nanostructures physically mediate cross-taxa interference.

Vesicular influence on population dynamics is strictly stoichiometric. At baseline physiological ratios, EVs facilitated anaerobic denitrification and early recipient growth, putatively via metabolic enzyme supplementation. Crossing a critical density threshold, however, inverted this dynamic. High EV concentrations exerted a dominant growth-inhibitory effect during the stationary phase following nitrate depletion. We hypothesize this terminal suppression emerges from the synergistic delivery of anaerobic effectors, primarily peptidoglycan hydrolases operating in tandem with hypoxically induced pyocins (Toyofuku et al., 2014). Admittedly, definitively isolating these specific proteinaceous targets as the exclusive drivers of growth arrest will necessitate future genetic validations, such as targeted gene knockouts. While similar inhibitory effects have also been found in aerobic cultures (Kadurugamuwa and Beveridge, 1996; Li et al., 1998), the bioenergetic constraints of anoxia amplify this phenotype. Comparable dose-dependent suppression occurs following high-titer EV exposure in *Escherichia coli* models (Kawagishi et al., 2025). These prior observations, however, map a strictly unidimensional trajectory: escalating vesicular concentrations dictate intensified cytotoxicity. Our data diverge fundamentally from this linear paradigm. We captured a stringent functional duality. Given the extreme molecular heterogeneity of the packaged proteome, this biphasic response completely reframes the ecological role of biogenic EVs. They function beyond mere static agents of mortality, operating instead as dynamic, density-dependent rheostats that continuously titrate community metabolism against prevailing environmental constraints.

Inducing localized mortality among kin within densely packed, resource-depleted spatial structures, initially appears counterintuitive. We propose that the ensuing gradual membrane permeabilization after cell death likely facilitates a slow exudation of intracellular carbon and nitrogen pools. This passive leakage cross-feeds the surviving community matrix. By reallocating these resources, the overall fitness of the community is maintained particularly under anaerobic denitrification, where canonical quorum sensing is suppressed (Lee et al., 2011), highlighting its potential as a complementary social mechanism. Tracing dynamic nutrient fluxes and recipient multi-omics *in vivo* will be strictly necessary to validate this resource reallocation model.

Recipient physiological state heavily dictates susceptibility to these vesicular effectors. In aerobic denitrification, cells simultaneously respire both oxygen and nitrate, engaging two distinct electron transport chains (Chen et al., 2006). This metabolic flexibility supports robust and stable growth, potentially enabling cells to better withstand or compensate for external perturbations—including the addition of exogenous EVs. In contrast, under anaerobic denitrification, cells are constrained to a single, less efficient energy-generating pathway and must cope with the cumulative stresses of energy limitation and

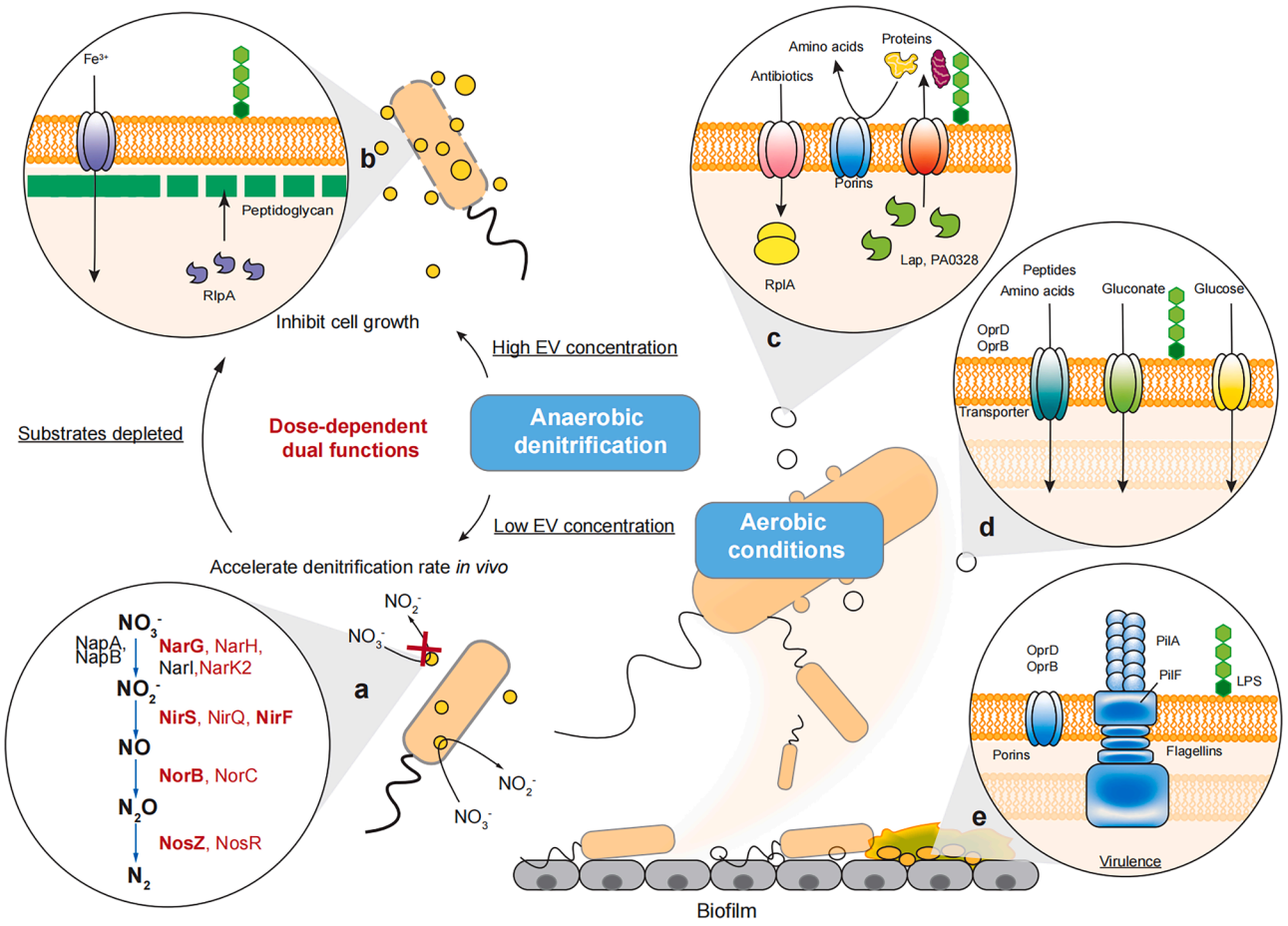


Fig. 6. Proposed conceptual model for condition-specific biogenesis and function of extracellular vesicles (EVs) in *Pseudomonas aeruginosa* PAO1. Environmental factors (O_2 and NO_3^-) regulate EV production, size, and protein cargo. Under anaerobic denitrifying condition, cells produce more and larger EVs, which exhibit dose-dependent functional duality in microbial ecology. **a.** Metabolic support at low EV concentration. Anaerobic denitrifying EVs carry key denitrifying enzymes. At low, physiologically relevant concentration, these EVs enhance denitrification rate in recipient cells during co-culture. However, they show no nitrate reduction activity *in vitro*, suggesting a role in intercellular metabolic support rather than independent catalysis. **b.** Population control at high EV concentration. The same EVs are enriched with lytic transglycosylase (e.g., RlpA), at high concentration or after nitrate depletion, these EVs may induce explosive cell lysis and release more EVs release upon interaction with susceptible cells, thereby limiting population density. **c-e.** Aerobic EVs: nutrient scavenging, stress resistance and virulence. EVs produced under aerobic conditions are enriched in porins and proteases. These may facilitate nutrient acquisition by hydrolyzing extracellular proteins and importing amino acids. Porins may also contribute to stress resistance and surface adhesion. As structural components of outer membrane, all EV populations carry lipopolysaccharide (LPS) and other immunogenic molecules. EVs from Aerobic denitrifying carry elevated levels of flagellins and additional virulence factors, which could help host cell adhesion, biofilm formation, and immune activation (e.g., LPS-induced reactive oxygen species and mucin production from airway epithelial cells in cystic fibrosis).

nitrosative stress (Chayabutra and Ju, 2000). In this more vulnerable physiological state, the same EV challenge may be sufficient to trigger measurable growth inhibition. This framework suggests that the observed functional impact of EVs is not solely determined by EV cargo, but also by the physiological context of the recipient cells.

Notably, despite packaging a nearly complete set of denitrification enzyme—likely reflecting their high expression levels in parent cells (Kamath et al., 2017)—purified EVs were catalytically inactive *in vitro*, even when provided with an electron donor (NADH). This finding, corroborated by our use of highly purified EVs through density gradient centrifugation, challenges the paradigm of EVs as independent metabolic entities. Instead, our data strongly support a model where EVs primarily function as carriers for targeted effector delivery, with their enzymatic cargo requiring the context of a recipient cell for functional manifestation. This clarifies apparent conflicts with previous studies that may have used less stringent purification protocols (Dauros Singorenko et al., 2017; Tian et al., 2020).

The stoichiometric dose-dependency and condition-specific proteomic sorting detailed here derive exclusively from the model denitrifier *P. aeruginosa* PAO1. While this highly tractable organism provides an optimal baseline for resolving the fundamental biophysics of anaerobic vesiculation, its physical responses cannot singularly represent the vast phylogenetic diversity of environmental denitrifiers. Consequently, the vesicular duality established in this study—shifting from metabolic facilitation to cytotoxic interference—currently serves as a foundational, model-derived hypothesis (Fig. 6) for broader ecological contexts. Verifying the universality of these dynamic colloidal interactions necessitates future investigations encompassing diverse environmental isolates and complex, multi-species denitrifying consortia.

Extending these principles beyond natural microbial ecology, the inherent physical resilience of these complex nanostructures poses distinct challenges in engineered environments. Our simulated municipal treatment assays revealed that nearly half of the biogenic nanoparticulate fraction withstands aggressive physicochemical oxidation. Identifying whether this loss is random or whether specific EV subpopulations (e.g., those with distinct size, density, or protein/lipid composition) are inherently more resistant, remains an open empirical question. While historical literature has explored the physical stability (Bomberger et al., 2009) and the cytotoxicity of enriched pathogen EVs (Takahara et al., 2024), assuming these extensively oxidized residual

particles retain comparable biological infectivity fundamentally lacks empirical basis. Future studies employing high-resolution sorting, proteomic characterization and empirical confirmation of pre- and post-treatment EVs will be necessary to identify potential markers of EV stability and evaluate its potential health risks to human being.

5. Conclusion

This study demonstrates that the opportunistic pathogen *P. aeruginosa* utilizes EVs as dynamic ecological regulators. The core findings and their environmental implications are summarized as follows:

- **Condition-specific functional diversification:** Environmental oxygen and nitrate availability strictly dictate EV composition. Aerobic conditions yield EVs enriched with virulence factors and nutrient acquisition, while anaerobic denitrification promotes the targeted packaging of peptidoglycan-degrading enzymes, serving as a mechanism for effector delivery or stress-induced cellular clearance.
- **Dose-dependent ecological duality:** EVs actively mediate bacterial population dynamics based on their local concentrations. At physiological ratios, they facilitate denitrification rates and cell growth. However, at higher concentrations or upon nutrient depletion, they transition into cytotoxic effectors that suppress population density, facilitating community-level nutrient recycling.
- **Biophysical resilience in engineered infrastructure:** Purified biogenic EVs exhibit remarkable physical recalcitrance against sequential, multi-barrier municipal water treatment cascades. Surviving intensive physical interception, physicochemical adsorption, and chemical oxidation, a substantial colloidal fraction remains structurally intact. This robust physical persistence redefines these vesicular structures as highly recalcitrant environmental biocolloids, shifting the focus of future water purification evaluations toward nanoscale colloidal attenuation.

CRediT authorship contribution statement

Yuzhen Ming: Conceptualization, Formal analysis, Investigation, Methodology, Visualization, Writing – original draft, Writing – review & editing. **Wengen Zhu:** Formal analysis, Investigation. **Huanping Liu:** Formal analysis. **Zuyuan Gao:** Investigation. **Shiwei Xiao:** Investigation. **Lanlan Cai:** Writing – review & editing. **Xuyan He:** Formal analysis. **Yusong Guo:** Writing – review & editing. **Jizhong Zhou:** Writing – review & editing. **Zhili He:** Writing – review & editing. **Qinglu Zeng:** Conceptualization, Methodology, Supervision, Writing – review & editing. **Qingyun Yan:** Conceptualization, Methodology, Project administration, Supervision, Writing – review & editing.

Declaration of competing interest

The authors declare that they have no known competing financial interests or personal relationships that could have appeared to influence the work reported in this paper.

Acknowledgments

We would like to express our gratitude to Professor Jingyun Fang from the School of Environmental Science and Engineering at Sun Yat-Sen University for valuable guidance on drinking water purification treatment. The work is supported by the National Natural Science Foundation of China (42377111), the Southern Marine Science and Engineering Guangdong Laboratory (Zhuhai) (SML2024SP002, SML2024SP022), the Ocean Negative Carbon Emissions (ONCE) Program and the Guangdong Provincial Basic and Applied Basic Research Fund Regional Joint Fund Project (2025B515130001).

Supplementary materials

Supplementary material associated with this article can be found, in the online version, at doi:10.1016/j.watres.2026.126745.

Data availability

The proteomics data that support the findings of this study have been deposited to the ProteomeXchange Consortium with the dataset identifier PXD054578.

References

Arhin, A., Boucher, C., 2010. The outer membrane protein OprQ and adherence of *Pseudomonas aeruginosa* to human fibronectin. Microbiology 156 (5), 1415–1423. https://doi.org/10.1099/mic.0.033472-0.

Biller, S.J., Schubotz, F., Roggensack, S.E., Thompson, A.W., Summons, R.E., Chisholm, S.W., 2014. Bacterial vesicles in marine ecosystems. Science 343 (6167), 183–186. https://doi.org/10.1126/science.1243457.

Bomberger, J.M., MacEachran, D.P., Coutermarsh, B.A., Ye, S., O'Toole, G.A., Stanton, B. A., 2009. Long-distance delivery of bacterial virulence factors by *Pseudomonas aeruginosa* outer membrane vesicles. PLOS Pathog 5 (4), e1000382. https://doi.org/10.1371/journal.ppat.1000382.

Brito, I.L., 2021. Examining horizontal gene transfer in microbial communities. Nat. Rev. Microbiol. 19 (7), 442–453. https://doi.org/10.1038/s41579-021-00534-7.

Chayabutra, C., Ju, L.-K., 2000. Degradation of N-hexadecane and its metabolites by *Pseudomonas aeruginosa* under microaerobic and anaerobic denitrifying conditions. Appl. Environ. Microbiol. 66 (2), 493–498. https://doi.org/10.1128/AEM.66.2.493-498.2000.

Cheluvappa, R., Shimmon, R., Dawson, M., Hilmer, S.N., Le Couteur, D.G., 2008. Reactions of *Pseudomonas aeruginosa* pyocyanin with reduced glutathione. Acta Biochim. Pol. 55 (3), 571–580. https://doi.org/10.18388/abp.2008_3063.

Chen, F., Xia, Q., Ju, L.-K., 2006. Competition between oxygen and nitrate respirations in continuous culture of *Pseudomonas aeruginosa* performing aerobic denitrification. Biotechnol. Bioeng. 93 (6), 1069–1078. https://doi.org/10.1002/bit.20812.

Cheng, X., Chen, Z., Gao, C., Zhang, Y., Yang, L., Wan, J., Wei, Y., Zeng, S., Zhang, Y., Zhang, Y., Li, Y., Zhang, W., Zou, Q., Lu, G., Gu, J., 2023. Structural and biological insights into outer membrane protein lipotoxin F of *Pseudomonas aeruginosa*: implications for vaccine application. Int. J. Biol. Macromol. 253, 127634. https://doi.org/10.1016/j.ijbiomac.2023.127634.

Chevalier, S., Bouffartigues, E., Bodilis, J., Maillot, O., Lesouhaitier, O., Feuilloley, M.G. J., Orange, N., Dufour, A., Cornelis, P., 2017. Structure, function and regulation of *Pseudomonas aeruginosa* porins. FEMS Microbiol. Rev. 41 (5), 698–722. https://doi.org/10.1093/femsre/fux020.

Chung, J., Amin, K., Kim, S., Yoon, S., Kwon, K., Bae, W., 2014. Autotrophic denitrification of nitrate and nitrite using thiosulfate as an electron donor. Water Res. 58, 169–178. https://doi.org/10.1016/j.watres.2014.03.071.

Dauros Singorenko, P., Chang, V., Whitcombe, A., Simonov, D., Hong, J., Phillips, A., Swift, S., Blenkiron, C., 2017. Isolation of membrane vesicles from prokaryotes: a technical and biological comparison reveals heterogeneity. J. Extracell. Vesicles 6 (1), 1324731. https://doi.org/10.1080/20013078.2017.1324731.

Farinha, M.A., Ronald, S.L., Kropinski, A.M., Paranchych, W., 1993. Localization of the virulence-associated genes *pilA, pilR, rpoN, fliA, fliC, Ent*, and *Fbp* on the physical map of *Pseudomonas aeruginosa* PAO1 by pulsed-field electrophoresis. Infect. Immun. 61 (4), 1571–1575. https://doi.org/10.1128/iai.61.4.1571-1575.1993.

Feitosa-Junior, O.R., Stefanello, E., Zaini, P.A., Nascimento, R., Pierry, P.M., Dandekar, A.M., Lindow, S.E., da Silva, A.M., 2019. Proteomic and metabolomic analyses of *Xylella fastidiosa* OMV-enriched fractions reveal association with virulence factors and signaling molecules of the DSF family. Phytopathology 109 (8), 1344–1353. https://doi.org/10.1094/PHYTO-03-19-0083-R.

Fonseka, P., Mathivanan, S., 2023. Extracellular vesicles biogenesis, cargo sorting and implications in disease conditions. Cells 12 (2), 280. https://doi.org/10.3390/cells12020280.

Gamper, M., Zimmermann, A., Haas, D., 1991. Anaerobic regulation of transcription initiation in the *arcDABC* operon of *Pseudomonas aeruginosa*. J. Bacteriol. 173 (15), 4742–4750. https://doi.org/10.1128/jb.173.15.4742-4750.1991.

Gill, S., Catchpole, R., Forterre, P., 2019. Extracellular membrane vesicles in the three domains of life and beyond. FEMS Microbiol. Rev. 43 (3), 273–303. https://doi.org/10.1093/femsre/fuy042.

Huang, H., Hancock, R.E., 1993. Genetic definition of the substrate selectivity of outer membrane porin protein OprD of *Pseudomonas aeruginosa*. J. Bacteriol. 175 (24), 7793–7800. https://doi.org/10.1128/jb.175.24.7793-7800.1993.

Iraci, N., Gaude, E., Leonardi, T., Costa, A.S.H., Cossetti, C., Peruzzotti-Jametti, L., Bernstock, J.D., Saini, H.K., Gelati, M., Vescovi, A.L., Bastos, C., Faria, N., Occhipinti, L.G., Enright, A.J., Frezza, C., Pluchino, S., 2017. Extracellular vesicles are independent metabolic units with asparaginase activity. Nat. Chem. Biol. 13 (9), 951–955. https://doi.org/10.1038/nchembio.2422.

Jones, P., Binns, D., Chang, H.-Y., Fraser, M., Li, W., McAnulla, C., McWilliam, H., Maslen, J., Mitchell, A., Nuka, G., Pesseat, S., Quinn, A.F., Sangrador-Vegas, A., Scheremetjew, M., Yong, S.-Y., Lopez, R., Hunter, S., 2014. InterProScan 5: genome-scale protein function classification. Bioinformatics 30 (9), 1236–1240. https://doi.org/10.1093/bioinformatics/btu031.

Jorgenson, M.A., Chen, Y., Yahashiri, A., Popham, D.L., Weiss, D.S., 2014. The bacterial septal ring protein RlpA is a lytic transglycosylase that contributes to rod shape and daughter cell separation in *Pseudomonas aeruginosa*. Mol. Microbiol. 93 (1), 113–128. https://doi.org/10.1111/mmi.12643.

Kadurugamuwa, J.L., Beveridge, T.J., 1996. Bacteriolytic effect of membrane vesicles from *Pseudomonas aeruginosa* on other bacteria including pathogens: conceptually new antibiotics. J. Bacteriol. 178 (10), 2767–2774. https://doi.org/10.1128/jb.178.10.2767-2774.1996.

Kamath, K.S., Krisp, C., Chick, J., Pascovici, D., Gygi, S.P., Molloy, M.P., 2017. *Pseudomonas aeruginosa* proteome under hypoxic stress conditions mimicking the cystic fibrosis lung. J. Proteome Res. 16 (10), 3917–3928. https://doi.org/10.1021/acs.jproteome.7b00561.

Kang, E.H., Gebru, E., Kim, M.H., Cheng, H., Park, S.-C., 2009. EstA protein, a novel virulence factor of *Streptococcus pneumoniae*, induces nitric oxide and pro-inflammatory cytokine production in RAW 264.7 macrophages through NF-κB/MAPK. Microb. Pathog. 47 (4), 196–201. https://doi.org/10.1016/j.micpath.2009.07.002.

Kawagishi, Y., Murase, K., Grebenshchikova, A., Iibushi, J., Ma, C., Kimeu, T.M., Minowa-Nozawa, A., Nozawa, T., Nakagawa, I., 2025. Bacterial extracellular vesicles target different bacterial species, impairing cell division and diminishing their pathogenicity. Proc. Natl. Acad. Sci. 122 (18), e2416652122. https://doi.org/10.1073/pnas.2416652122.

Koo, J., Tammam, S., Ku, S.-Y., Sampaleanu, L.M., Burrows, L.L., Howell, P.L., 2008. PilF is an outer membrane lipoprotein required for multimerization and localization of the Pseudomonas *aeruginosa* type IV pilus secretin. J. Bacteriol. 190 (21), 6961–6969. https://doi.org/10.1128/jb.00996-08.

Kuypers, M.M.M., Marchant, H.K., Kartal, B., 2018. The microbial nitrogen-cycling network. Nat. Rev. Microbiol. 16 (5), 263–276. https://doi.org/10.1038/nrmicro.2018.9.

Lee, K.M., Yoon, M.Y., Park, Y., Lee, J.-H., Yoon, S.S., 2011. Anaerobiosis-induced loss of cytotoxicity is due to inactivation of quorum sensing in *Pseudomonas aeruginosa*. Infect. Immun. 79 (7), 2792–2800. https://doi.org/10.1128/iai.01361-10.

Li, Z., Clarke, A.J., Beveridge, T.J., 1998. Gram-negative bacteria produce membrane vesicles which are capable of killing other bacteria. J. Bacteriol. 180 (20), 5478–5483. https://doi.org/10.1128/jb.180.20.5478-5483.1998.

Manning, A.J., Kuehn, M.J., 2011. Contribution of bacterial outer membrane vesicles to innate bacterial defense. BMC Microbiol. 11 (1), 258. https://doi.org/10.1186/1471-2180-11-258.

Maphosa, S., Moleleki, L.N., Motaung, T.E., 2023. Bacterial secretion system functions: evidence of interactions and downstream implications. Microbiology 169 (4), 001326. https://doi.org/10.1099/mic.0.001326.

Marchant, H.K., Ahmerkamp, S., Lavik, G., Tegetmeyer, H.E., Graf, J., Klatt, J.M., Holtappels, M., Walpersdorf, E., Kuypers, M.M.M., 2017. Denitrifying community in coastal sediments performs aerobic and anaerobic respiration simultaneously. ISME J. 11 (8), 1799–1812. https://doi.org/10.1038/ismej.2017.51.

Morinaga, K., Yamamoto, T., Nomura, N., Toyofuku, M., 2018. *Paracoccus denitrificans* can utilize various long-chain n-acyl homoserine lactones and sequester them in membrane vesicles. Environ. Microbiol. Rep. 10 (6), 651–654. https://doi.org/10.1111/1758-2229.12674.

Nascimento, R., Gouran, H., Chakraborty, S., Gillespie, H.W., Almeida-Souza, H.O., Tu, A., Rao, B.J., Feldstein, P.A., Bruening, G., Goulart, L.R., Dandekar, A.M., 2016. The type II secreted lipase/esterase LesA is a key virulence factor required for *Xylella fastidiosa* pathogenesis in grapevines. Sci. Rep. 6 (1), 18598. https://doi.org/10.1038/srep18598.

Orench-Rivera, N., Kuehn, M.J., 2016. Environmentally controlled bacterial vesicle-mediated export. Cell Microbiol. 18 (11), 1525–1536. https://doi.org/10.1111/cmi.12676.

Pal, S., Jain, D., Biswal, S., Rastogi, S.K., Kumar, G., Ghosh, A.S., 2024. The physiological role of *Acinetobacter baumannii* DacC is exerted through influencing cell shape, biofilm formation, the fitness of survival, and manifesting DD-carboxypeptidase and beta-lactamase dual-enzyme activities. FEMS Microbiol. Lett. 371, fnae079. https://doi.org/10.1093/femsle/fnae079.

Quinn, J.P., Darzins, A., Miyashiro, D., Ripp, S., Miller, R.V., 1991. Imipenem resistance in *Pseudomonas aeruginosa* PAO: mapping of the OprD2 gene. Antimicrob. Agents Chemother. 35 (4), 753–755. https://doi.org/10.1128/aac.35.4.753.

Rebière-Huët, J., Guérillon, J., Pimenta, A.L., Di Martino, P., Orange, N., Hulen, C., 2002. Porins of *Pseudomonas fluorescens* MFO as fibronectin-binding proteins. FEMS Microbiol. Lett. 215 (1), 121–126. https://doi.org/10.1016/S0378-1097(02)00920-5.

Renelli, M., Matias, V., Lo, R.Y., Beveridge, T.J., 2004. DNA-containing membrane vesicles of *Pseudomonas aeruginosa* PAO1 and their genetic transformation potential. Microbiology 150 (7), 2161–2169. https://doi.org/10.1099/mic.0.26841-0.

Salvachúa, D., Werner, A.Z., Pardo, I., Michalska, M., Black, B.A., Donohoe, B.S., Haugen, S.J., Katahira, R., Notonier, S., Ramirez, K.J., Amore, A., Purvine, S.O., Zink, E.M., Abraham, P.E., Giannone, R.J., Poudel, S., Laible, P.D., Hettich, R.L., Beckham, G.T., 2020. Outer membrane vesicles catabolize lignin-derived aromatic compounds in *Pseudomonas putida* KT2440. Proc. Natl. Acad. Sci 117 (17), 9302–9310. https://doi.org/10.1073/pnas.1921073117.

Schatz, D., Schleyer, G., Saltvedt, M.R., Sandaa, R.-A., Feldmesser, E., Vardi, A., 2021. Ecological significance of extracellular vesicles in modulating host-virus interactions during algal blooms. ISME J. 15 (12), 3714–3721. https://doi.org/10.1038/s41396-021-01018-5.

Sherman, B.T., Hao, M., Qiu, J., Jiao, X., Baseler, M.W., Lane, H.C., Imamichi, T., Chang, W., 2022. DAVID: a web server for functional enrichment analysis and functional annotation of gene lists (2021 update). Nucleic Acids Res. 50 (W1), W216–W221. https://doi.org/10.1093/nar/gkac194.

Solé, M., Scheibner, F., Hoffmeister, A.-K., Hartmann, N., Hause, G., Rother, A., Jordan, M., Lautier, M., Arlat, M., Büttner, D., 2015. *Xanthomonas campestris* pv. *vesicatoria* secretes proteases and xylanases via the Xps type II secretion system and outer membrane vesicles. J. Bacteriol. 197 (17), 2879–2893. https://doi.org/10.1128/jb.00322-15.

Takahara, M., Hirayama, S., Futamata, H., Nakao, R., Tashiro, Y., 2024. Biofilm-derived membrane vesicles exhibit potent immunomodulatory activity in *Pseudomonas aeruginosa* PAO1. Microbiol. Immunol. 68 (7), 224–236. https://doi.org/10.1111/1348-0421.13156.

Tamber, S., Maier, E., Benz, R., Hancock, R.E.W., 2007. Characterization of OpdH, a *Pseudomonas aeruginosa* porin involved in the uptake of tricarboxylates. J. Bacteriol. 189 (3), 929–939. https://doi.org/10.1128/jb.01296-06.

Tashiro, Y., Ichikawa, S., Shimizu, M., Toyofuku, M., Takaya, N., Nakajima-Kambe, T., Uchiyama, H., Nomura, N., 2010. Variation of physiochemical properties and cell association activity of membrane vesicles with growth phase in *Pseudomonas aeruginosa*. Appl. Environ. Microbiol. 76 (11), 3732–3739. https://doi.org/10.1128/aem.02794-09.

Thomas, K.L., Lloyd, D., Boddy, L., 1994. Effects of oxygen, pH and nitrate concentration on denitrification by *Pseudomonas* species. FEMS Microbiol. Lett. 118 (1–2), 181–186. https://doi.org/10.1111/j.1574-6968.1994.tb06823.x.

Tian, Y., Gong, M., Hu, Y., Liu, H., Zhang, W., Zhang, M., Hu, X., Aubert, D., Zhu, S., Wu, L., Yan, X., 2020. Quality and efficiency assessment of six extracellular vesicle isolation methods by nano-flow cytometry. J. Extracell. Vesicles 9 (1), 1697028. https://doi.org/10.1080/20013078.2019.1697028.

Tkach, M., Théry, C., 2016. Communication by extracellular vesicles: where we are and where we need to go. Cell 164 (6), 1226–1232. https://doi.org/10.1016/j.cell.2016.01.043.

Toyofuku, M., Cárcamo-Oyarce, G., Yamamoto, T., Eisenstein, F., Hsiao, C.-C., Kurosawa, M., Gademann, K., Pilhofer, M., Nomura, N., Eberl, L., 2017. Prophage-triggered membrane vesicle formation through peptidoglycan damage in *Bacillus subtilis*. Nat. Commun. 8 (1), 481. https://doi.org/10.1038/s41467-017-00492-w.

Toyofuku, M., Nomura, N., Eberl, L., 2019. Types and origins of bacterial membrane vesicles. Nat. Rev. Microbiol. 17 (1), 13–24. https://doi.org/10.1038/s41579-018-0112-2.

Toyofuku, M., Schild, S., Kaparakis-Liaskos, M., Eberl, L., 2023. Composition and functions of bacterial membrane vesicles. Nat. Rev. Microbiol. 21 (7), 415–430. https://doi.org/10.1038/s41579-023-00875-5.

Toyofuku, M., Zhou, S., Sawada, I., Takaya, N., Uchiyama, H., Nomura, N., 2014. Membrane vesicle formation is associated with pyocin production under denitrifying conditions in *Pseudomonas aeruginosa* PAO1. Environ. Microbiol. 16 (9), 2927–2938. https://doi.org/10.1111/1462-2920.12260.

Trias, J., Nikaido, H., 1990. Protein D2 channel of the *Pseudomonas aeruginosa* outer membrane has a binding site for basic amino acids and peptides. J. Biol. Chem. 265 (26), 15680–15684. https://doi.org/10.1016/S0021-9258(18)55452-1.

Turnbull, L., Toyofuku, M., Hynen, A.L., Kurosawa, M., Pessi, G., Petty, N.K., Osvath, S. R., Cárcamo-Oyarce, G., Gloag, E.S., Shimoni, R., Omasits, U., Ito, S., Yap, X., Monahan, L.G., Cavaliere, R., Ahrens, C.H., Charles, I.G., Nomura, N., Eberl, L., Whitchurch, C.B., 2016. Explosive cell lysis as a mechanism for the biogenesis of bacterial membrane vesicles and biofilms. Nat. Commun. 7 (1). https://doi.org/10.1038/ncomms11220.

Ucar, D., Zhang, Y., Angelidaki, I., 2017. An overview of electron acceptors in microbial fuel cells. Front. Microbiol. 8. https://doi.org/10.3389/fmicb.2017.00643.

Vanaja, S.K., Russo, A.J., Behl, B., Banerjee, I., Yankova, M., Deshmukh, S.D., Rathinam, V.A.K., 2016. Bacterial outer membrane vesicles mediate cytosolic localization of LPS and caspase-11 activation. Cell 165 (5), 1106–1119. https://doi.org/10.1016/j.cell.2016.04.015.

Vander Wauven, C., Piérard, A., Kley-Raymann, M., Haas, D., 1984. *Pseudomonas aeruginosa* mutants affected in anaerobic growth on arginine: evidence for a four-gene cluster encoding the arginine deiminase pathway. J. Bacteriol. 160 (3), 928–934. https://doi.org/10.1128/jb.160.3.928-934.1984.

Wang, Z., Zhou, X., Kong, Q., He, H., Sun, J., Qiu, W., Zhang, L., Yang, M., 2024. Extracellular vesicle preparation and analysis: a state-of-the-art review. Adv. Sci. 11 (30), 2401069. https://doi.org/10.1002/advs.202401069.

Webber, J., Clayton, A., 2013. How pure are your vesicles? J. Extracell. Vesicles 2 (1), 19861. https://doi.org/10.3402/jev.v2i0.19861.

Wylie, J.L., Worobec, E.A., 1995. The OprB porin plays a central role in carbohydrate uptake in *Pseudomonas aeruginosa*. J. Bacteriol. 177 (11), 3021–3026. https://doi.org/10.1128/jb.177.11.3021-3026.1995.

Xie, J., Li, Q., Haesebrouck, F., Hoecke, L.V., Vandenbroucke, R.E., 2022. The tremendous biomedical potential of bacterial extracellular vesicles. Trends Biotechnol 40 (10), 1173–1194. https://doi.org/10.1016/j.tibtech.2022.03.005.

Yang, J., Feng, L., Pi, S., Cui, D., Ma, F., Zhao, H., Li, A., 2020. A critical review of aerobic denitrification: insights into the intracellular electron transfer. Sci. Total Environ. 731, 139080. https://doi.org/10.1016/j.scitotenv.2020.139080.

Yoneyama, H., Yamano, Y., Nakae, T., 1995. Role of porins in the antibiotic susceptibility of *Pseudomonas aeruginosa*: construction of mutants with deletions in the multiple porin genes. Biochem. Biophys. Res. Commun. 213 (1), 88–95. https://doi.org/10.1006/bbrc.1995.2102.

Zarantonello, V., Silva, T.P., Noyma, N.P., Gamalier, J.P., Mello, M.M., Marinho, M.M., Melo, R.C.N., 2018. The cyanobacterium *Cylindrospermopsis raciborskii* (CYRF-01) responds to environmental stresses with increased vesiculation detected at single-cell resolution. Front. Microbiol. 9. https://doi.org/10.3389/fmicb.2018.00272.

Zhang, D., Li, M., Yang, Y., Yu, H., Xiao, F., Mao, C., Huang, J., Yu, Y., Wang, Y., Wu, B., Wang, C., Shu, L., He, Z., Yan, Q., 2022. Nitrite and nitrate reduction drive sediment microbial nitrogen cycling in a eutrophic lake. Water Res. 220, 118637. https://doi.org/10.1016/j.watres.2022.118637.